

Discrete memristive conservative chaotic map: dynamics, hardware implementation and application in secure communication

Quanli Deng, Chunhua Wang, Yichuang Sun *Senior Member, IEEE*, Gang Yang

Abstract—The randomness of chaotic systems are crucial for their application in secure communication. Conservative systems exhibit enhanced ergodicity and randomness in comparison to dissipative chaotic systems. However, the memristor-based conservative chaotic maps remain unreported. This paper presents a study of volume-preserving chaotic maps based on discrete memristor (DM). We propose and analyze a generic conservative map that incorporates DM. The conservative characteristics of the proposed iterative map are confirmed through the determinant of its Jacobian matrix. Furthermore, four distinct DM models are introduced and their memristive characteristics are verified through numerical simulations of hysteresis loops. To investigate the dynamical properties of the discrete memristive conservative map (DMCM), we incorporate the proposed DM models into the generic conservative map model using numerical methods, including phase portraits, Lyapunov exponents, and bifurcation diagrams. Additionally, the hardware implementation of the DMCM on an FPGA platform demonstrates the reliability of the model. Finally, secure communication experiments based on the DMCM show that it outperforms some classical dissipative chaotic maps in terms of bit error rate performance.

Index Terms—conservative chaos, discrete memristor, FPGA implementation, secure communication.

I. INTRODUCTION

CHAOTIC systems exhibit several unique properties, such as sensitivity to initial conditions, topological transitivity, and a dense distribution of periodic orbits. These characteristics have inspired extensive research across various academic fields and have facilitated applications in a broad range of industrial domains [1]–[3]. Generally, chaotic systems can be categorized into two types: dissipative and conservative. Dissipative systems gradually lose energy over time and tend to converge towards attractors, whereas conservative systems conserve energy, are unable to form attractors, and maintain a constant phase volume. In comparison to dissipative systems,

conservative systems may offer advantages in terms of randomness and ergodicity [4]. Strong randomness is crucial for the reliability of applying chaos in fields such as image encryption and secure communication [5]–[7].

Memristors have a wide range of applications in recent years, including in-memory computing [8]–[10], bio-inspired circuits [11]–[13], and chaotic systems [14]–[16], contributing significantly to advancements in these fields. The conservative chaotic oscillations cooperating with memristors in the continuous-time systems have attracted considerable interest. Zhang *et al.* delved into memristor-based conservative systems, revealing symmetrical dynamics across varying control parameters and initial conditions [17]. Du *et al.* further contributed by constructing a non-Hamiltonian conservative system leveraging a charge-controlled memristor, exploring both heterogeneous and homogeneous multistability within the chaotic system [18]. Li *et al.* introduced a novel memristor-based conservative chaotic system exhibiting extreme multistability and hyperchaos properties [19]. These conservative chaotic systems exhibit enhanced ergodicity and randomness than the dissipative chaotic systems.

The current research primarily focuses on establishing memristive conservative systems in the continuous-time domain. In contrast, discrete-time systems offer several advantages, including more convenient hardware implementation, faster computation capabilities and enhancing dynamical complexity [20], [21]. Given these benefits, exploring memristive chaotic maps with in discrete-time domain holds significant importance. Bao *et al.* introduced a circuit model incorporating a sampling switch, a memristor, and a capacitor. They employed the discrete Euler algorithm to construct a discrete-time iterative map and explored the chaotic characteristics of the model through various numerical simulations [22]. Fu *et al.* proposed a novel approach, utilizing the difference in state variables as input to the memristor to formulate a memristor-based Hénon map model. Based on this, they subsequently designed an iterative map using analog circuits [23]. To tackle the challenges of discontinuous chaotic intervals and low Lyapunov exponents in chaotic maps, Lai *et al.* presented a memristor-based hyperchaotic map capable of generating cubic attractors and exhibiting ultra-boosting behaviors, thereby effectively enhancing the complexity of the chaotic system [24]. These efforts have introduced innovative techniques for enhancing the dynamical characteristics of chaotic maps through the integration of memristors into discrete-time iterative maps.

Manuscript received Month xx, 2xxx; revised Month xx, xxxx; accepted Month x, xxxx. This work was supported in part by the National Natural Science Foundation of China under Grant 62271197, and in part by the Guangdong Basic and Applied Basic Research Foundation under Grant 2024A1515011910.

Quanli Deng, Chunhua Wang, and Gang Yang are with the College of Information Science and Engineering, Hunan University, Changsha, 410082, China (Corresponding author: Chunhua Wang, e-mail: wch1227164@hnu.edu.cn).

Chunhua Wang is also with the Greater Bay Area Institute for Innovation, Hunan University, Guangzhou, 511300, China.

Yichuang Sun is with the School of Engineering and Computer Science, University of Hertfordshire, Hatfield AL10 9AB, U.K.

However, it is noteworthy that these memristive chaotic maps are dissipative systems, conservative memristive maps remains unreported.

Recognizing the potential superiority of conservative chaotic systems and the benefits of integrating memristors into discrete maps, we delve into the exploration of the conservative map incorporated with the discrete-time memristors. To this end, we design a generic discrete memristive conservative map (DMCM). The conservative property of the DMCM is analyzed by examining the determinant of its Jacobian matrix. To gain insights into the dynamical behaviors, we employ four distinct discrete memristor models as case studies. A comprehensive numerical simulation of these dynamics is conducted, encompassing various perspectives such as phase portraits, Lyapunov exponents (LEs), bifurcation diagrams (BDs), and attraction basin. The primary contributions of this article are outlined as follows.

1) A generic discrete memristive conservative system is proposed, and its dynamic characteristics are revealed using four distinct memristor models as case studies.

2) A hardware implementation of the DMCM is designed, leveraging the Field-Programmable Gate Array (FPGA) platform.

3) A secure communication system based on conservative chaotic flows is designed and evaluated. Our findings demonstrate that the proposed scheme based on DMCM outperforms some classical dissipative chaotic maps in terms of performance.

The remainder of this study is organized as follows. Section II describes generic DMCM model and four distinct discrete memristor models. Section III investigates the dynamical behaviors of the DMCM by four different memristor models. Section IV focuses on the digital implementation using FPGA technology. Section V designs the chaotic secure communication scheme and evaluates its performance. Finally, Section VI summarizes the whole work and provides further research directions.

II. MODEL DESCRIPTION

A. Generic DM-based conservative map model

Given the distinctive nonlinear characteristics of DMs, these models have been utilized for the generation of chaotic maps. In this work, we introduce a novel DM-based conservative map, wherein the DM serves as a nonlinear component within the discrete-time iterative system, as depicted in Fig.1. Within this framework, z^{-1} denotes a one sampling step delay of the state variable. The parameters m and k represent the control parameters of the state variable y_n self-feedback and the memristive feedback, respectively. Furthermore, $M(z_n)$ denotes the resistance function of the DM.

With the schematic structure illustrated in Fig.1, a generic DM-based conservative map can be formulated as follows:

$$\begin{cases} x_{n+1} = y_n \\ y_{n+1} = -x_n - kM(z_n)y_n + my_n \\ z_{n+1} = z_n + f(y_n) \end{cases} \quad (1)$$

where x_{n+1} is the $(n+1)$ -th value of the state variable x , which is set to the n -th value of state variable y . The new value of

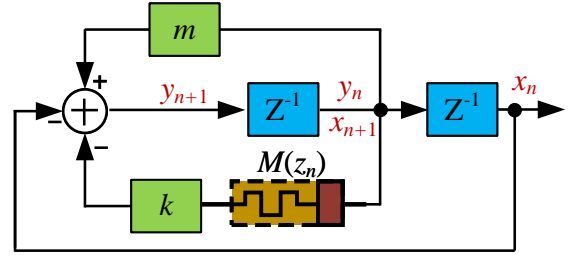


Fig. 1. Structure of the DM-based conservative chaotic map model.

state variable y at the $(n+1)$ -th iteration, y_{n+1} , is determined by the current state variable x_n , self-feedback with control parameter m , and memristive feedback with control parameter k . The state variable of the DM at the $(n+1)$ -th iteration is denoted as z_{n+1} , which is determined by the n -th value of itself, and the state variable y_n .

The conservative characteristic of the system (1) implies that the determinant of the Jacobian matrix should equal to one, indicating that the system preserves the volume in the state space during its evolution. The Jacobian matrix of the DM-based map can be derived as follows:

$$\mathbf{J} = \begin{bmatrix} 0 & 1 & 0 \\ -1 & m - kM(z_n) & -kM'(z_n)y_n \\ 0 & f'(y_n) & 1 \end{bmatrix} \quad (2)$$

where $M'(z_n)$ and $f'(y_n)$ represent the derivative functions of $M(z_n)$ and $f(y_n)$, respectively.

Obviously, the determinant of the above matrix can be obtained by

$$\det(\mathbf{J}) = (-1)^{1+2} \cdot (-1) \begin{vmatrix} 1 & 0 \\ f'(y_n) & 1 \end{vmatrix} = 1 \quad (3)$$

Consequently, the dynamics of the proposed map is a conservative map [25].

B. Discrete memristor models

According to their mathematical expressions, memristors can be classified into three categories including ideal memristor, generic memristor and extended memristor. The mathematical definition of the generic memristor model is shown as

$$\begin{aligned} v &= M(x)i \\ dx/dt &= f(x, i) \end{aligned} \quad (4)$$

where $M(x)$ denotes the resistance value of the memristor that depends on the state variable x , and the function $f(x, i)$ represents the relationship between the state variable x and the input i .

Inspired by the work [22], a discrete generic memristor can be obtained by performing the forward Euler method on the model (4). The mathematical definition of the discrete generic memristor can be obtained as

$$\begin{aligned} v_n &= M(x_n)i_n \\ x_{n+1} &= x_n + f(x_n, i_n) \end{aligned} \quad (5)$$

where i_n , v_n and x_n are the input, output and state variable at the n -th sampling time. In this study, four different forms of

discrete generic memristor model are designed as shown in (6). These models are developed using a trial-and-error approach, with the objective of constructing conservative maps in the subsequent design process.

$$\text{DM1: } \begin{cases} v_n = \tanh(x_n)i_n \\ x_{n+1} = x_n + i_n \cdot \exp(-i_n^2) \end{cases} \quad (6a)$$

$$\text{DM2: } \begin{cases} v_n = \tanh(x_n)i_n \\ x_{n+1} = x_n + \exp(-0.2(i_n - 3)^2) \\ \quad - \exp(-0.2(i_n + 3)^2) \end{cases} \quad (6b)$$

$$\text{DM3: } \begin{cases} v_n = \cos(\pi x_n)i_n \\ x_{n+1} = x_n + (\tanh(i_n) - \text{sign}(i_n)) \\ \quad \cdot (1 - \cos(i_n)) \end{cases} \quad (6c)$$

$$\text{DM4: } \begin{cases} v_n = (x_n \cdot \exp(-x_n^2))i_n \\ x_{n+1} = x_n + \tanh(2i_n) - \tanh(i_n) \end{cases} \quad (6d)$$

Drawing upon the test scheme outlined in [22], we conduct a hysteresis loop analysis in the i_n - v_n plane by connecting a discrete current source to the input terminal of the DM models. Specifically, we utilize a discrete sinusoidal current signal denoted as $i_n = 0.5\sin(\omega n)$, where n represents the discrete time index. By varying the frequency ω , we numerically simulate the resulting current-voltage relationship using MATLAB and present the outcomes in Fig.2. The results reveal that all four DM models exhibit pinched hysteresis loops in the i_n - v_n plane. Furthermore, as the frequency ω increases, the area enclosed by the hysteresis loop lobes decreases monotonically. These numerical results conclusively demonstrate that these four DM models possess the characteristics of memristors.

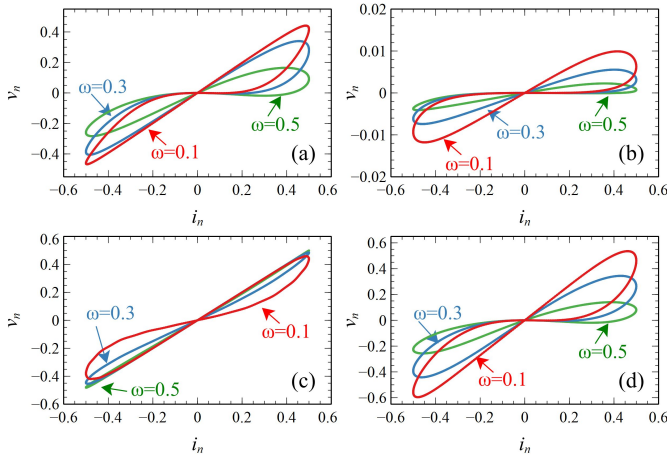


Fig. 2. Frequency-dependent pinched hysteresis loops when applying $i_n=0.5\sin(\omega n)$ to (a) DM1 model, (b) DM2 model, (c) DM3 model, (d) DM4 model.

III. NUMERICAL SIMULATION RESULTS

By substituting the various forms of DM models provided in (6) into the generic DM-based conservative map model (1), we obtain four distinct DMCMs as (7).

$$\text{DMCM1: } \begin{cases} x_{n+1} = y_n \\ y_{n+1} = -x_n - k \tanh(z_n)y_n + my_n \\ z_{n+1} = z_n + y_n \cdot \exp(-y_n^2) \end{cases} \quad (7a)$$

$$\text{DMCM2: } \begin{cases} x_{n+1} = y_n \\ y_{n+1} = -x_n - k \tanh(z_n)y_n + my_n \\ z_{n+1} = z_n + \exp(-0.2(y_n - 3)^2) \\ \quad - \exp(-0.2(y_n + 3)^2) \end{cases} \quad (7b)$$

$$\text{DMCM3: } \begin{cases} x_{n+1} = y_n \\ y_{n+1} = -x_n - k \cos(\pi z_n)y_n + my_n \\ z_{n+1} = z_n + (\tanh(y_n) - \text{sign}(y_n)) \\ \quad \cdot (1 - \cos(y_n)) \end{cases} \quad (7c)$$

$$\text{DMCM4: } \begin{cases} x_{n+1} = y_n \\ y_{n+1} = -x_n - k(z_n \cdot \exp(-z_n^2))y_n + my_n \\ z_{n+1} = z_n + \tanh(2y_n) - \tanh(y_n) \end{cases} \quad (7d)$$

To investigate the dynamical properties of these DMCMs, we analyze them from the aspects, including the phase portraits, Lyapunov exponents, bifurcation diagrams, and attraction basins.

A. Phase plots of the DMCMs

With the memristive feedback parameter k set to 1, the self-feedback control parameter m set to 0.4, and initial values of 1, 0, 0, we perform numerical iterations 10^5 times on the MATLAB for the four distinct DMCMs. The resulting chaotic flows are projected onto the $x - y$ plane, as depicted in Fig.3. Unlike dissipative chaotic systems, which typically exhibit strange attractors that compress motion into a lower-dimensional set, the trajectories of conservative systems generally remain within the full-dimensional phase space and do not converge to a lower-dimensional manifold. Through observations of the phase portraits, it can be seen that the DMCMs possess the properties of conservative chaotic systems.

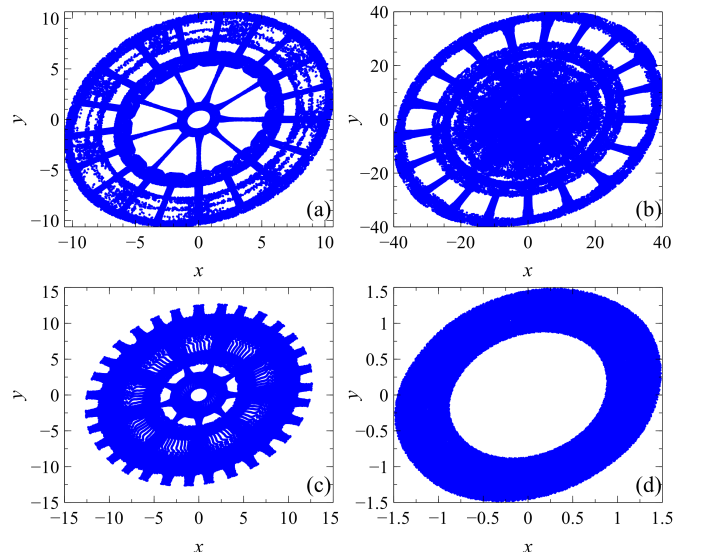


Fig. 3. Chaotic flows projected on $x - y$ plane with $k=1$, $m=0.4$ for (a) DMCM1, (b) DMCM2, (c) DMCM3, (d) DMCM4.

In dissipative continuous systems, a chaotic attractor is typically indicated by a largest Lyapunov exponent (LLE) greater than zero and a sum of all LEs less than zero. In dissipative discrete chaotic systems, chaos is primarily characterized by a positive LLE, while the sum of LEs can be either positive or negative. In contrast, for conservative systems, the sum of all LEs must equal zero. The numerical calculated results for the four distinct DMCMs are summarized in Table I. These results show that the DMCMs have LEs with a sum of zero and exhibit integer dimensions. This confirms that the DMCMs possess the characteristics of conservative chaotic systems. The Kaplan-Yorke dimension (D_{KY}) provides additional information about the dimensionality of the chaotic flow in these systems.

TABLE I
LEs AND KAPLAN-YORKE DIMENSIONS OF DMCMs

| models | LE1 | LE2 | LE3 | $\sum LEs$ | D_{KY} |
|--------|--------|---------|---------|------------|----------|
| DMCM1 | 0.0087 | -0.0002 | -0.0085 | 0 | 3 |
| DMCM2 | 0.0052 | 0.0001 | -0.0053 | 0 | 3 |
| DMCM3 | 0.0388 | -0.0001 | -0.0387 | 0 | 3 |
| DMCM4 | 0.0052 | -0.0001 | -0.0051 | 0 | 3 |

B. Parameter-dependent dynamical behaviors

With the self-feedback parameter m fixed at 0.4 and initial conditions set to 1, 0, 0, we explore the influence of the memristive feedback strength k on the dynamics of the four distinct DMCMs through the Lyapunov exponent spectra. Figs.4 (a) to (d) show the LEs with respect to the parameter k in the range $[-1,1]$ for each DMCM. As can be seen in Figs.4(a1) to (d1), the positive LE and the negative LE are symmetrical about the y -axis at zero. The sums of LEs for each DMCM have been plotted in Figs.4(a2) to (d2), and the resulting lines coincide with the y -axis at zero conforming that the systems are conservative. When the absolute value of k is small, all the LEs equal to zero, indicating that DMCMs exhibit quasi-periodic behavior. As the parameter k increases beyond a certain threshold, a positive LE emerges, indicating that the DMCM transitions into the chaotic state.

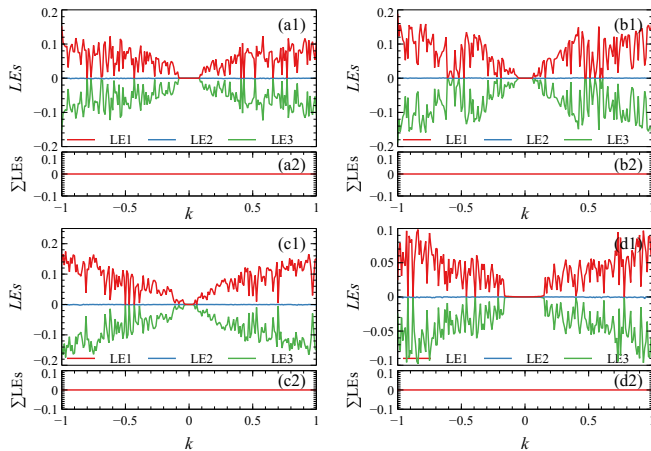


Fig. 4. Lyapunov exponents spectra with $k \in [-1,1]$ for (a) DMCM1 (b) DMCM2 (c) DMCM3 (d) DMCM4.

The bifurcation behavior of the state variable x for the four DMCMs is illustrated in Fig.5. The symmetry properties of the state variable x can be disclosed from the bifurcation diagrams. In particular, the conservative chaotic orbit arises from a quasi-periodic bifurcation, which is a specific bifurcation route compared to the more common period-doubling bifurcation [26].

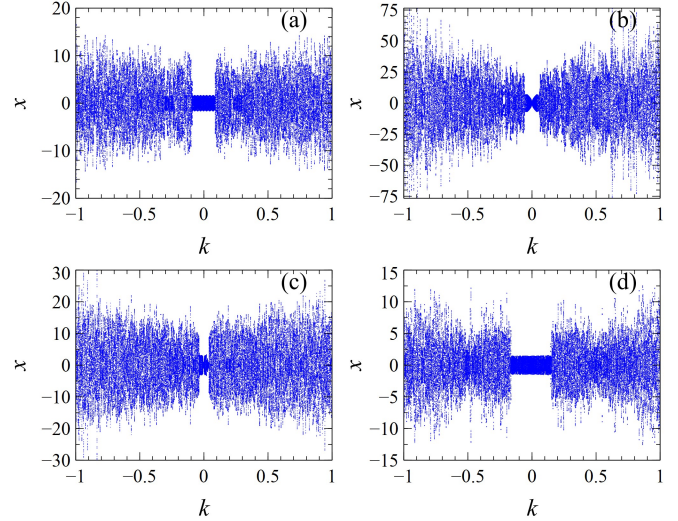


Fig. 5. Bifurcation diagram of x with $k \in [-1,1]$ for (a) DMCM1 (b) DMCM2 (c) DMCM3 (d) DMCM4.

The influence of the self-feedback strength m on the dynamics of the four distinct DMCMs is explored through the LEs by setting $k=0.1$ and the initial conditions to 1, 0, 0. As the self-feedback strength m varies in the range $[-1,1]$, the LEs of the systems exhibit symmetry about $y=0$, as shown in Fig.6(a1) to (d1). The sum of all LEs for each DMCM equals to zero, satisfying the characteristic of conservative systems. The LE spectra show unique patterns that reflect the specific dynamics of each DMCM with the variation of m . For example, in the case of DMCM1, there are three positive LLE parameter intervals $[-0.78,-0.23]$, $[0.35,0.42]$ and $[0.53,0.95]$. Comparing the variations of LEs with the bifurcation behavior of the state x in Fig.7, the bifurcation behavior influenced by m is corresponding to the variations of LEs. This correspondence reveals the dynamical variations that occur as the self-feedback strength varies.

C. Initial condition-dependent dynamical behaviors

In the realm of nonlinear systems, certain systems can exhibit multiple distinct dynamical behavior in response to variations in initial conditions. This phenomenon, known as coexistence of dynamical behaviors, has been extensively studied in dissipative systems, particularly in the context of coexistence of multiple attractors. Although conservative chaotic systems cannot form attractors, coexistence phenomena still exist in conservative systems. The coexisting flows can also be found by setting different initial values. The system can display multiple stable dynamical behaviors, which persist over time. Fix the parameters of DMCMs as $k=0.1$ and $m=0.4$.

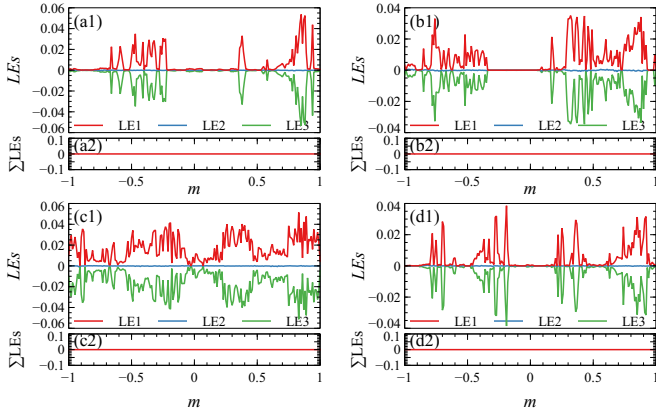


Fig. 6. Lyapunov exponents spectra with $m \in [-1,1]$ for (a) DMCM1 (b) DMCM2 (c) DMCM3 (d) DMCM4.

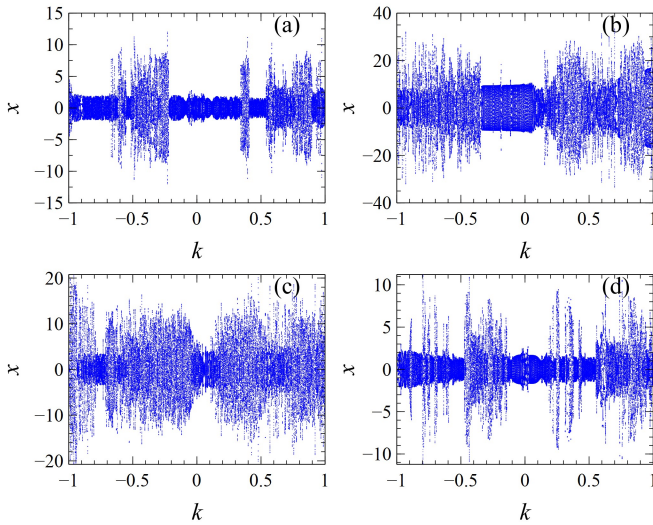


Fig. 7. Bifurcation diagram of x with $m \in [-1,1]$ for (a) DMCM1 (b) DMCM2 (c) DMCM3 (d) DMCM4.

Varying the initial condition of state variable x in range $[-4,4]$, Fig.8 depicts the LE spectra with respect to the variation of initial condition. As can be observed the LLE can take value of zero or positive numbers, indicating that changes in the initial condition lead to the dynamical behavior variations of DMCMs.

As an illustration, Fig.9 depicts the phase portraits of the co-existing flows of DMCM1, corresponding to initial conditions $[0.01,0,0]$ and $[1,0,0]$. In Fig.9(a), the red region indicates the periodic behavior, while in Fig.9(b), the blue region represents the chaotic behavior. The attraction basin is known as a set of all initial conditions in the phase space that lead to a specific flow as time progresses, which essentially defines the region in the state space from which the trajectory will be converged. Set the initial value of the state variable z to 0. The attraction basin is obtained by changing the values of x_0 and y_0 in range $[-4,4]$, as shown in Fig.10. The coexisted bistable flows are painted by distinct colors, where the blue represents the initial regions converge to the quasi-periodic flow, and the yellow denotes a chaotic flow can be obtained by selecting initial

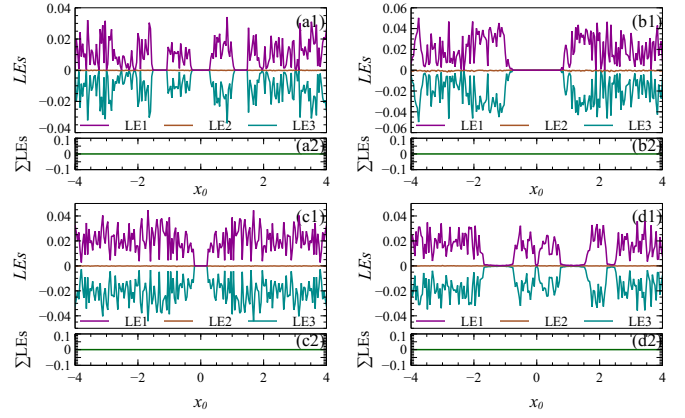


Fig. 8. Lyapunov exponents spectra with $x_0 \in [-4,4]$ for (a) DMCM1 (b) DMCM2 (c) DMCM3 (d) DMCM4.

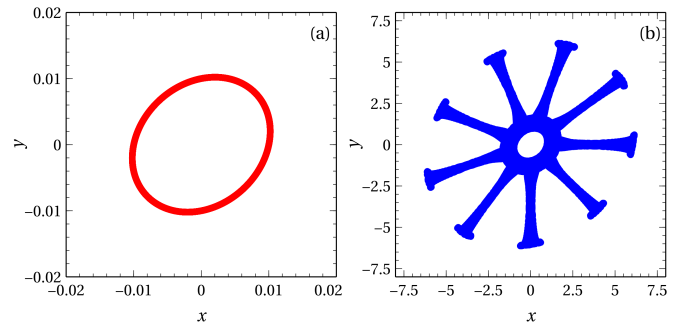


Fig. 9. Coexisted phase portraits in DMCM1 with initial conditions for (a) $[0.01,0,0]$ (b) $[1,0,0]$.

values in these areas. The attraction basins reveal the complex dynamics behaviors of the DMCMs depending on the initial conditions.

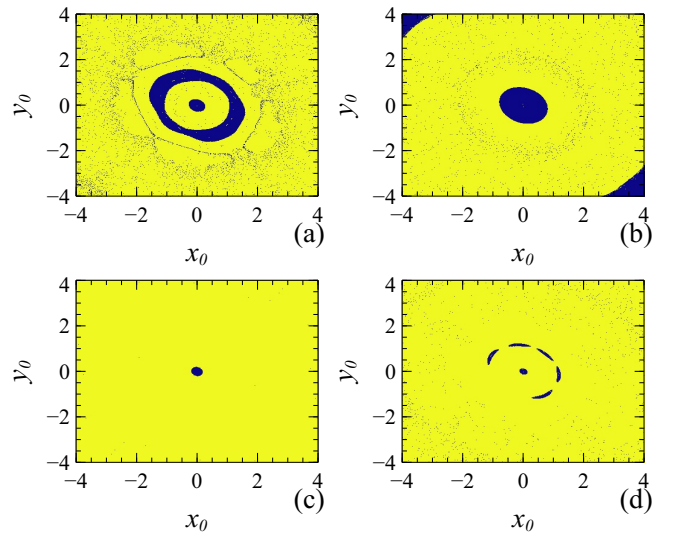


Fig. 10. Attraction basin in x_0-y_0 plane for (a) DMCM1 (b) DMCM2 (c) DMCM3 (d) DMCM4.

IV. FPGA PLATFORM-BASED IMPLEMENTATION

The implementation of chaotic maps in FPGA-based digital circuits has garnered significant interest due to the advantages, such as high computational speed, robust stability, and the ease altering system parameters and initial conditions [27]–[29]. This study presents the FPGA-based implementation of the proposed DMCMs. The flow block diagram for the FPGA-based implementation of the DMCM models is shown in Fig.11. In this implementation, the state variables at the n -th iteration are denoted as xn , yn and zn , respectively. The DMCM block is responsible for performing the iterative calculations of the models, and the outcomes are transmitted to the Data Transfer block for preparation of the output signal for the Digital-to-Analog Converter (DAC). The iterative calculations and output preparation operations are executed on the Xilinx xc7z020clg400-1 platform. The digital signals are then converted into analog singles by the AD9767 DAC and subsequently captured using an oscilloscope.

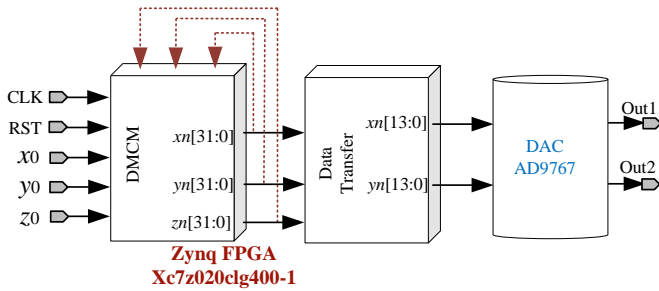


Fig. 11. Block diagram for the FPGA-based implementation of DMCMs.

In the FPGA-based design process, the Verilog Hardware Digital Language is utilized to craft the program code. A 32-bit fixed-point decimal format, comprised of 1 sign bit, 6 integer bits, and 25 decimal bits, is employed for precision. The hyperbolic tangent function is achieved through an approximation technique as delineated in [30]. For the implementation of cosine function in the FPGA, the CORDIC algorithm is implemented using the Verilog HDL. The implementation of the exponential function facilitates the transformation of the exponential function with base e into one with base 2 for computation purposes as proposed in [31].

The hardware experimental results, with the initial conditions for the state variables xn , yn and zn set to 1, 0, 0, respectively, and parameters as $k=0.1$, $m=0.4$, are depicted in Fig.12. Observations from the hardware implemented phase portraits in $xn - yn$ plane, as captured by the oscilloscope, aligns with the numerical simulations presented in Fig.3. These experimental results demonstrate the feasibility and simplicity of digital FPGA-based implementation, and also manifest the correctness of the mathematical models of DMCMs.

V. APPLICATION IN SECURE COMMUNICATION

Chaotic systems are prime candidates for secure communication due to their inherent properties, including unpredictability and ergodicity [32]–[34]. Conservative chaotic systems often exhibit enhanced ergodicity and randomness compared to

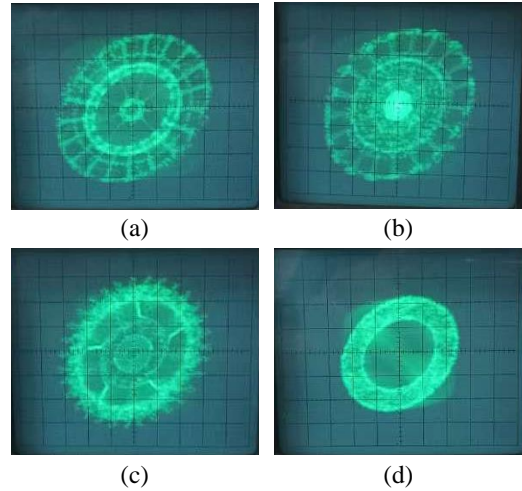


Fig. 12. Captured results on oscilloscope of FPGA-based implementation for (a) DMCM1, (b) DMCM2, (c) DMCM3, (d) DMCM4.

dissipative chaos. Consequently, conservative chaotic maps are well-suited for secure communication applications. We integrate DMCMs into the reference-shifted differential chaos shift keying (RS-DCSK) [35] communication scheme to showcase the utility of DMCMs in secure communications.

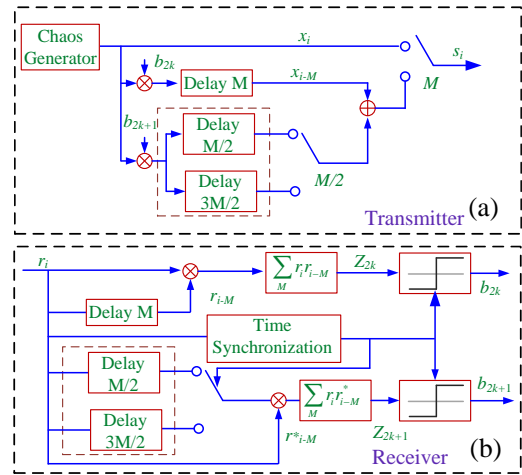


Fig. 13. Schematic of the RS-DCSK for (a) transmitter (b) receiver.

The RS-DCSK represents a non-coherent system that eliminates the need for synchronized chaotic carriers [36], making it an attractive and practical choice for real-world applications. In the transmitter of RS-DCSK system, as illustrated in Fig.13(a), each frame consists of two equal time slots: the first slot is dedicated to transmitting a chaotic reference signal, while the second slot carries the information-bearing signal. Both an exact copy and a shifted version of the signal transmitted in the first slot serve as message bearers, allowing each wavelet in the second time slot to convey two bits of information. The k -th frame of the transmitted signal $s_i(k)$ can be derived using

the following equation

$$s_i(k) = \begin{cases} x_i & 2kM < i \leq (2k+1)M \\ \frac{(b_{2k}x_{i-M} + b_{2k+1}x_{i-M/2})}{\sqrt{2}} & (2k+1)M < i \leq (2k+1.5)M \\ \frac{(b_{2k}x_{i-M} + b_{2k+1}x_{i-3M/2})}{\sqrt{2}} & (2k+1.5)M < i \leq 2(k+1)M \end{cases} \quad (8)$$

where b_{2k} and b_{2k+1} represent the information bits contained within the k -th frame. The chaotic sequence of length M , denoted as $x_{2kM+1} \dots x_{(2k+1)M}$, serves as the reference for b_{2k} . The reference for b_{2k+1} is obtained by circularly right shifting the reference of b_{2k} by $M/2$ times, a process that is executed within the delay block depicted in Fig.13(a).

The schematic structure for recovering the information bits is illustrated in Fig.13(b). This structure employs two independent branches to identify every bit simultaneously but separately. To extract information bits, the received signal r_i is multiplied by its delayed signal r_{i-M} and r_{i-M}^* respectively in two branches. The signal r_{i-M}^* is obtained by circularly left shifting r_{i-M} for $M/2$. Assuming perfect bit synchronization has been established and the received signal r_i is described by $r_i = s_i + \xi_i$ where ξ_i represents the channel noise, the outputs Z_{2k} and Z_{2k+1} for b_{2k} and b_{2k+1} can be calculated using the following equations

$$Z_{2k} = \sum_{i=(2k+1)M}^{2(k+1)M} r_{i-M} r_i \quad (9)$$

$$= \frac{b_{2k}}{\sqrt{2}} \sum_{i=(2k+1)M}^{2(k+1)M} x_{i-M}^2 + \gamma$$

$$Z_{2k+1} = \sum_{i=(2k+1)M}^{2(k+1)M} r_{i-M}^* r_i \quad (10)$$

$$= \frac{b_{2k+1}}{\sqrt{2}} \sum_{i=(2k+1)M}^{2(k+1)M} x_{i-M}^2 + \eta$$

where γ and η are the noise components. The information bits of b_{2k} and b_{2k+1} are recovered by the sign of Z_{2k} and Z_{2k+1} , which can be calculated by

$$\hat{b}_n = \begin{cases} 1 & Z_n > 0 \\ -1 & Z_n \leq 0. \end{cases} \quad (11)$$

Given that most physical transmission channels are subject to Gaussian noise, we simulate the RS-DCSK system in an additive white Gaussian noise (AWGN) environment and calculate the bit error rate (BER) under various signal-noise-rate (SNR) and spread factors. In these experiments, the state x after modulo 1 calculation of the discrete memristive conservative chaotic maps is utilized as the chaos generator. The modulo operation regulates the state variable in region $[0,1]$, which facilitates the comparison with subsequent dissipative systems whose output range are also within $[0,1]$. The parameters (k,m) for each DMCMs are set to $(0.1,0.4)$. These parameter settings guarantee that all the discrete maps exhibit chaotic behavior.

Two sets of experiments are designed to evaluate the BERs using randomly generated sequences of length 5^4 bits. The first set of experiments examines the BERs against varying

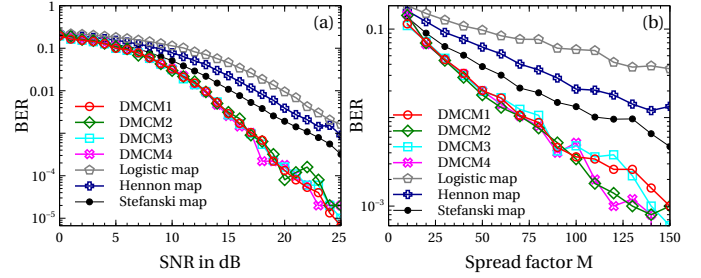


Fig. 14. BERs of the RS-DCSK using different chaotic maps when (a) spread factor $M=40$ and noise strength SNR varying in $[0,25]$ (b) SNR=10 and M varying in $[10,150]$

levels of noise. Specifically, the RS-DCSK system is simulated ten times using randomly generated initial states for each simulation, with the spread factor M fixed at 40 and the SNR varied in the range of $[0,25]$ dB. The average BERs from these ten simulations are then calculated. The simulated results are presented in Fig.14(a). It can be seen that all the chaotic maps achieve similar BERs under the high noise conditions. However, as the SNR increases, the schemes based on memristive conservative maps achieve significantly lower BERs compared to the three classical dissipative chaotic systems. The second set of experiments investigate the BERs against different lengths of the spread factor M . Specifically, the SNR of noisy signal is fixed to 10 dB, and the spread factor M is varied within the range of $[10,150]$. The BERs are calculated ten times for each value of M , with randomly generated initial values for the DMCMs. The average BERs from these ten simulations are then computed. The experimental results are plotted in Fig.14(b). For the purpose of comparison, we selected the one-dimensional Logistic map, the two-dimensional Hennon map and the three-dimensional Stefanski map. These classical chaotic maps are all dissipative systems. It can be observed that the RS-DCSK system using the presented memristive conservative maps achieves much lower BERs compared to the system using the three classical dissipative chaotic maps. Based on the results concerning performance against noise, it can be concluded that the discrete memristive conservative chaotic maps are more suitable for the secure communication application than some one-dimensional dissipative maps.

VI. CONCLUSION AND OUTLOOK

Conservative chaotic systems, as an important branch of nonlinear systems, have not yet received sufficient attention, especially regarding the study of discrete-time conservative maps. While previous works [17]–[19] have explored continuous-time memristive conservative systems requiring computationally expensive integral operations. Investigating of discrete-time memristive conservative system cannot only revealing dynamical behaviors in discrete-time domain but also lay a foundation for conservative chaos-based applications. This work makes three key advances: (1) We present a novel discrete memristive conservative map for the first time that eliminates the need for numerical integration while preserving essential conservative properties; (2) Compared to the analog

implementations in [17]–[19], our FPGA-based digital realization achieves faster iteration speed and provide a foundation for subsequent hardware-oriented research. (3) The developed secure communication scheme based on conservative chaotic flows achieves lower bit error rate compared to some classical dissipative chaotic maps. These innovations bridge the gap between theoretical conservative dynamics and practical digital applications.

Future research will focus on three promising directions: (1) extending this framework to explore other discrete-time memory elements such as memcapacitor-based conservative systems, which reveal new dynamical phenomena; (2) designing more complex discrete-time memristive conservative systems with multiple positive LEs and developing corresponding chaos control strategies; and (3) investigating practical industrial applications of conservative chaotic flows, particularly in secure communication and signal processing domains. These directions could significantly expand both theoretical understanding and practical implementation of conservative nonlinear systems.

REFERENCES

- [1] Q. Lai, L. Yang, G. Hu, Z.-H. Guan, and H. H.-C. Iu, “Constructing multiscroll memristive neural network with local activity memristor and application in image encryption,” *IEEE Transactions on Cybernetics*, vol. 54, no. 7, pp. 4039–4048, 2024.
- [2] Q. Deng, C. Wang, Y. Sun, Z. Deng, and G. Yang, “Memristive tabu learning neuron generated multi-wing attractor with FPGA implementation and application in encryption,” *IEEE Transactions on Circuits and Systems I: Regular Paper*, vol. 72, no. 1, pp. 300–311, 2025.
- [3] W. Feng, J. Zhang, Y. Chen, Z. Qin, Y. Zhang, M. Ahmad, and M. Wozniak, “Exploiting robust quadratic polynomial hyperchaotic map and pixel fusion strategy for efficient image encryption,” *Expert Systems with Applications*, vol. 246, p. 123190, 2024.
- [4] M. Ji’e, H. Peng, S. Duan, L. Wang, F. Zhang, and D. Yan, “Design and FPGA implementation of grid-scroll hamiltonian conservative chaotic flows with a line equilibrium,” *IEEE Transactions on Very Large Scale Integration (VLSI) Systems*, vol. 32, no. 4, pp. 658–668, 2024.
- [5] W. Feng, Z. Qin, J. Zhang, and M. Ahmad, “Cryptanalysis and improvement of the image encryption scheme based on feistel network and dynamic DNA encoding,” *IEEE Access*, vol. 9, pp. 145 459–145 470, 2021.
- [6] H. Lin, X. Deng, F. Yu, and Y. Sun, “Grid multibutterfly memristive neural network with three memristive systems: Modeling, dynamic analysis, and application in police IoT,” *IEEE Internet of Things Journal*, vol. 11, no. 18, pp. 29 878–29 889, 2024.
- [7] X. Kong, F. Yu, W. Yao, S. Cai, J. Zhang, and H. Lin, “Memristor-induced hyperchaos, multiscroll and extreme multistability in fractional-order HNN: Image encryption and FPAG implementation,” *Neural Networks*, vol. 171, pp. 85–103, 2024.
- [8] Q. Deng, C. Wang, J. Sun, Y. Sun, J. Jiang, H. Lin, and Z. Deng, “Nonvolatile CMOS memristor, reconfigurable array, and its application in power load forecasting,” *IEEE Transactions on Industrial Informatics*, vol. 20, no. 4, pp. 6130–6141, 2024.
- [9] Q. Deng, C. Wang, and Z. Deng, “Memristive circuit of quaternion multiplication and its application in aircraft attitude computation,” *IEEE Transactions on Circuits and Systems II: Express Briefs*, vol. 71, no. 8, pp. 3970–3974, 2024.
- [10] H. Xiao, X. Hu, T. Gao, Y. Zhou, S. Duan, and Y. Chen, “Efficient low-bit neural network with memristor-based reconfigurable circuits,” *IEEE Transactions on Circuits and Systems II: Express Briefs*, vol. 71, no. 1, pp. 66–70, 2024.
- [11] J. Sun, Y. Zhai, P. Liu, and Y. Wang, “Memristor-based neural network circuit of operant conditioning with bridging and conditional reinforcement,” *IEEE Transactions on Circuits and Systems I: Regular Papers*, vol. 71, no. 8, pp. 3514–3525, 2024.
- [12] Z. Deng, C. Wang, H. Lin, Q. Deng, and Y. Sun, “Memristor-based attention network for online real-time object tracking,” *IEEE Transactions on Computer-Aided Design of Integrated Circuits and Systems*, vol. 44, no. 2, pp. 682–695, 2025.
- [13] Z. Chen, X. Wang, Z. Wang, C. Yang, T. Huang, J. Lai, and Z. Zeng, “A memristive spiking neural network circuit for bio-inspired navigation based on spatial cognitive mechanisms,” *IEEE Transactions on Biomedical Circuits and Systems*, vol. Early Access, 2024.
- [14] Q. Deng, C. Wang, Y. Sun, and G. Yang, “Memristive multi-wing chaotic Hopfield neural network for LiDAR data security,” *Nonlinear Dynamics*, vol. 113, pp. 17 161–17 176, 2025.
- [15] W. Feng, Q. Wang, H. Liu, Y. Ren, J. Zhang, S. Zhang, K. Qian, and H. Wen, “Exploiting newly designed fractional-order 3D Lorenz chaotic system and 2D discrete polynomial hyper-chaotic map for high-performance multi-image encryption,” *Fractal and Fractional*, vol. 7, no. 12, p. 887, 2023.
- [16] C. Wang, Y. Li, and Q. Deng, “Discrete-time fractional-order local active memristor-based Hopfield neural network and its FPGA implementation,” *Chaos, Solitons & Fractals*, vol. 193, p. 116053, 2025.
- [17] X. Zhang, C. Li, E. Dong, Y. Zhao, and Z. Liu, “A conservative memristive system with amplitude control and offset boosting,” *International Journal of Bifurcation and Chaos*, vol. 32, no. 4, p. 2250057, 2022.
- [18] C. Du, L. Liu, Z. Zhang, and S. Yu, “A conservative system based on a triangular wave memristor and its application in image encryption,” *Nonlinear Dynamics*, vol. 111, pp. 15 515–15 529, 2023.
- [19] Y. Li, M. Wang, H. Chang, H. Wang, and G. Chen, “A hyperchaotic memristive system with extreme multistability and conservativeness,” *Nonlinear Dynamics*, vol. 112, pp. 3851–3868, 2023.
- [20] Y. Wang, Z. Liu, L. Y. Zhang, F. Pareschi, G. Setti, and G. Chen, “From chaos to pseudorandomness: A case study on the 2-D coupled map lattice,” *IEEE Transactions on Cybernetics*, vol. 53, no. 2, pp. 1324–1334, 2023.
- [21] W. Deng and M. Ma, “Analysis of the dynamical behavior of discrete memristor-coupled scale-free neural networks,” *Chinese of Journal of Physics*, vol. 91, pp. 966–976, 2024.
- [22] B.-C. Bao, H. Li, H. Wu, X. Zhang, and M. Chen, “Hyperchaos in a second-order discrete memristor-based map model,” *Electronics Letters*, vol. 56, no. 15, pp. 769–770, 2020.
- [23] L. Fu, X. Wu, S. He, H. Wang, and K. Sun, “A memristive Hénon map based on the state variable difference and its analog circuit implementation,” *IEEE Transactions on Industrial Electronics*, vol. 71, no. 8, pp. 9668–9676, 2024.
- [24] Q. Lai, L. Yang, and G. Chen, “Design and performance analysis of discrete memristive hyperchaotic systems with stuffed cube attractors and ultraboosting behaviors,” *IEEE Transactions on Industrial Electronics*, vol. 71, no. 7, pp. 7819–7828, 2024.
- [25] H. Li, H. Bao, L. Zhu, B. Bao, and M. Chen, “Extreme multistability in simple area-preserving map,” *IEEE Access*, vol. 8, pp. 175 972–175 980, 2020.
- [26] H. Bao, Z. Chen, J. Ma, Q. Xu, and B. Bao, “Planar homogeneous coexisting hyperchaos in bi-memristor cyclic Hopfield neural network,” *IEEE Transactions on Industrial Electronics*, vol. 71, no. 12, pp. 16 398–16 408, 2024.
- [27] C. Wang, D. Luo, Q. Deng, and G. Yang, “Dynamics analysis and FPGA implementation of discrete memristive cellular neural network with heterogeneous activation functions,” *Chaos, Solitons & Fractals*, vol. 187, p. 115471, 2024.
- [28] F. Yu, X. Kong, W. Yao, J. Zhang, S. Cai, H. Lin, and J. Jin, “Dynamics analysis, synchronization and FPGA implementation of multiscroll Hopfield neural networks with non-polynomial memristor,” *Chaos, Solitons & Fractals*, vol. 179, p. 11440, 2024.
- [29] J. Mou, H. Cao, N. Zhou, and Y. Cao, “An FHN-HR neuron network coupled with a novel locally active memristor and its DSP implementation,” *IEEE Transactions on Cybernetics*, vol. 54, no. 12, pp. 7333–7342, 2024.
- [30] H. K. Kwan, “Simple sigmoid-like activation function suitable for digital hardware implementation,” *Electronics Letters*, vol. 28, pp. 1379–1380, 1992.
- [31] M. A. Hussain, S.-W. Lin, and T.-H. Tsai, “An area-efficient and high throughput hardware implementation of exponent function,” in *2022 IEEE International Symposium on Circuits and Systems (ISCAS)*, 2022, pp. 3369–3372.
- [32] M. Ma and Y. Lu, “Synchronization in scale-free neural networks under electromagnetic radiation,” *Chaos*, vol. 34, no. 3, p. 033116, 2024.
- [33] X. Ma, Z. Wang, and C. Wang, “An image encryption algorithm based on tabu search and hyperchaos,” *International Journal of Bifurcation and Chaos*, vol. 34, no. 14, p. 2450170, 2024.
- [34] C.-M. Lin, D.-H. Pham, and T.-T. Huynh, “Encryption and decryption of audio signal and image secure communications using chaotic system synchronization control by TSK fuzzy brain emotional learning

controllers,” *IEEE Transactions on Cybernetics*, vol. 52, no. 12, pp. 13 684–13 698, 2022.

- [35] H. Yang, G. Jiang, L. Xia, and X. Tu, “Reference-shifted DCSK modulation scheme for secure communication,” in *2017 International Conference on Computing, Networking and Communications (ICNC)*, 2017, pp. 1073–1076.
- [36] Z. Hua and Y. Zhou, “Exponential chaotic model for generating robust chaos,” *IEEE Transactions on Systems, Man, and Cybernetics: Systems*, vol. 51, no. 6, pp. 3713–3724, 2021.



Gang Yang received the B.S. degree in communications engineering and the M.S. degree in artificial intelligence from the Jiangxi University of science and technology, Ganzhou, China, in 2020 and 2023, respectively. He is currently working toward the Ph.D. degree with the College of Computer Science and Electronic Engineering, Hunan University, Changsha, China.

His current research interests include chaotic systems and circuits, memristor neural networks, and memristor systems and circuits.



Quanli Deng received the B.S. degree in microelectronics from the School of Physics and Optoelectronics, Xiangtan University, Xiangtan, China, in 2016, the M.S. in information and communication engineering from the College of Computer Science and Electronic Engineering, Hunan University, Changsha, China, in 2020 and the Ph.D. degree in computer science and technology from the College of Computer Science and Electronic Engineering, Hunan University, Changsha, China, in 2024.

He is currently a Postdoctoral Research Fellow with the College of Computer Science and Electronic Engineering, Hunan University. His research interests include modeling and analysis of neural systems, fundamental theory of nonlinear systems and circuits, and analog implementation of neuromorphic systems.



Chunhua Wang received the M.S. degree in microphysics from Zhengzhou University, Zhengzhou, China, in 1994, and the Ph.D. degree in microelectronics and solid-state electronics from the Beijing University of Technology, Beijing, China, in 2003.

He is currently a Professor with the College of Computer Science and Electronic Engineering, Hunan University, Changsha, China, where he is a Doctor Tutor and Director of the Advanced Communication Technology Key Laboratory. He has presided more than eight national and provincial projects and

authored or coauthored more than 200 papers retrieved by SCI, among which 20 papers were highly cited. His research interests include chaotic circuit, memristor circuit, chaotic encryption, neural networks based on memristor, complex networks, and current-mode circuit.

Dr. Wang is the Director of the Chaos and Nonlinear Circuit Professional Committee of Circuit and System Branch of the China Electronic Society.



Yichuang Sun (Senior Member, IEEE) received the B.Sc. and M.Sc. degrees from Dalian Maritime University, Dalian, China, in 1982 and 1985, respectively, and the Ph.D. degree from the University of York, York, U.K., in 1996, all in communications and electronics engineering.

Dr. Sun is currently Professor of Communications and Electronics, Head of Communications and Intelligent Systems Research Group, and Head of Electronic, Communication and Electrical Engineering Division in the School of Engineering and Computer

Science of the University of Hertfordshire, UK. He has published over 420 papers and contributed 10 chapters in edited books. He has also published four text and research books: *Continuous-Time Active Filter Design* (CRC Press, USA, 1999), *Design of High Frequency Integrated Analogue Filters* (IEE Press, UK, 2002), *Wireless Communication Circuits and Systems* (IET Press, 2004), and *Test and Diagnosis of Analogue, Mixed-signal and RF Integrated Circuits - the Systems on Chip Approach* (IET Press, 2008). His research interests are in the areas of wireless and mobile communications, RF and analogue circuits, memristor circuits and systems, and machine learning and neuromorphic computing.